

Effect of Li on the catalytic activity of MgO for the synthesis of flavanone

Jose A. Cortes-Concepcion, Florian Patcas, Michael D. Amiridis*

Department of Chemical Engineering, University of South Carolina, Columbia, SC 29208, United States

ARTICLE INFO

Article history:

Received 16 July 2009

Received in revised form 6 July 2010

Accepted 7 July 2010

Available online 15 July 2010

Keywords:

Lithium

Magnesium oxide

Flavanone synthesis

2'-Hydroxyacetophenone

Benzaldehyde

ABSTRACT

We have investigated the effects of Li on the structure, surface basicity and catalytic activity of MgO for the synthesis of flavanone. Introduction of low amounts of Li (i.e., ≤ 0.1 wt.%) was found to promote the rate of the Claisen–Schmidt condensation reaction, which is the first step in this process. However, at Li loadings above 0.1 wt.% a detrimental effect was observed, due to a concomitant decrease in surface area and increase in MgO crystallite size. A strong correlation was observed between surface-normalized basicity and catalytic activity. The increase in activity at higher levels of surface basicity can be attributed to the increased ability of Li–O[−] pairs to abstract a proton from the 2'-hydroxyacetophenone reactant, thus facilitating the adsorption and subsequent surface reactions of this molecule.

© 2010 Elsevier B.V. All rights reserved.

1. Introduction

Flavanone represents a significant intermediate in many pharmaceutical syntheses and members of the flavanoid family are attracting increased attention due to results of studies documenting their anticancer [1,2], anti-inflammatory [3–10], antibacterial [11,12], and anti-AIDS [13] pharmacological activity. Commercially, the synthesis of flavanone is carried out in a homogeneously catalyzed process, which combines the Claisen–Schmidt condensation of benzaldehyde and 2'-hydroxyacetophenone [14,15] and the subsequent isomerization of the 2'-hydroxychalcone intermediate formed to flavanone (Scheme 1). The feasibility of utilizing the same reaction steps to produce flavanone in a heterogeneously catalyzed system has been previously demonstrated by different groups, including our own [15–21].

The kinetics of this heterogeneous scheme for the synthesis of flavanone over MgO have been studied in detail in our group [17–19]. We have also investigated the reaction mechanism [16,20,22] and have developed a good understanding of the steps involved and the nature of the surface intermediates formed. However, there is still limited understanding of the nature of the active sites involved in this reaction, beyond some general notion of attributing the activity of MgO to its basicity [15].

This work is the continuation of our systematic investigation intended to address the nature of the active sites of MgO involved in the synthesis of flavanone, by adjusting its basic properties. In

a previous paper, the basicity of MgO was decreased in a controlled fashion, by selectively poisoning some of its basic sites by the introduction of different anions [23]. In this paper, by introducing lithium cations to MgO we attempted to increase its basicity and to produce a series of Li-modified MgO samples with different numbers and strengths of basic sites. The resulting catalysts were characterized by Temperature Programmed Desorption of CO₂ (CO₂-TPD), FTIR, XRD, BET, and HRTEM measurements. Subsequently, these samples were tested for their catalytic activity in the heterogeneous synthesis of flavanone and the results were correlated to those of the characterization measurements.

2. Experimental

2.1. Catalyst preparation

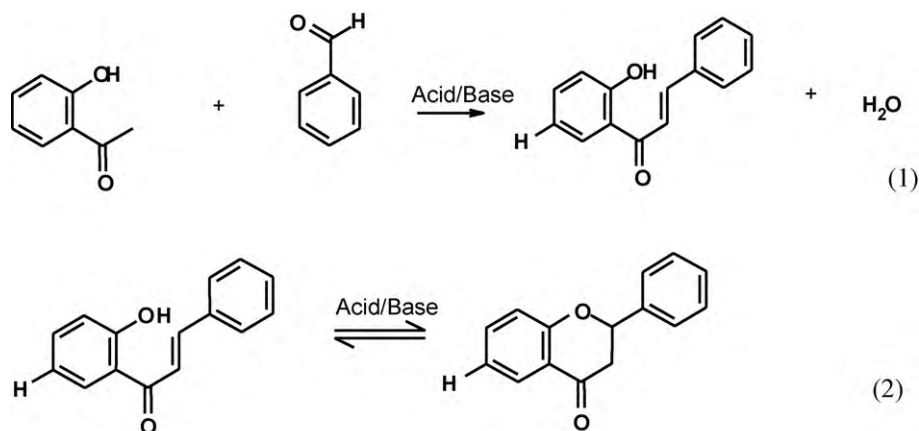
Samples containing different amounts of lithium were prepared via the addition of pure MgO (Aldrich, 99+% purity, $S_{\text{BET}} = 65 \text{ m}^2/\text{g}$) to an aqueous solution of lithium nitrate (Alfa Aesar, 99.99% metals basis). The resulting slurries were stirred at 353 K under atmospheric pressure until the water was evaporated. The materials obtained were subsequently calcined in air at 1023 K for 4 h.

2.2. Catalyst characterization

Surface areas of catalyst samples were determined by nitrogen adsorption at 77 K according to the BET multi-point method, using a Quantachrome Nova 1000e BET surface area analyzer.

X-ray diffraction (XRD) measurements were conducted using a Rigaku D/MAX-RB X-ray powder diffractometer, equipped with

* Corresponding author. Tel.: +1 803 777 7294; fax: +1 803 777 8265.
E-mail address: amiridis@cec.sc.edu (M.D. Amiridis).



Scheme 1. Flavanone synthesis via the Claisen–Schmidt condensation of 2'-hydroxyacetophenone with benzaldehyde (1) followed by the isomerization of the 2'-hydroxychalcone intermediate formed (2).

a graphite monochromator, operating at 40 kV and 50 mA, and a nickel-filtered Cu K α radiation source ($\lambda = 0.15406$ nm). Diffraction patterns were collected in the 5° to 70° (2θ) range at a scanning rate of $1.2^\circ \text{ min}^{-1}$. These XRD patterns were subsequently analyzed using the Jade v.7 software.

High resolution transmission electron microscopy (HRTEM) images were obtained with a Jeol 2000 FX microscope. In preparation for these measurements, powdered samples were dispersed on a dry copper grid coated with a carbon film.

CO₂ Temperature Programmed Desorption (CO₂-TPD) measurements were conducted with a Micromeritics Chemisorb 2750 instrument equipped with a TCD detector. Prior to their use, samples (50 mg) were treated in situ in He (UHP) at 1023 K for 1 h to remove any adsorbed contaminants. Subsequently, the samples were cooled down to room temperature in He, and were exposed to a 45% CO₂/He mixture (20 ml/min) for 30 min, followed by purging with pure He for 30 min. The temperature was then increased at a rate of 10 K/min from 298 to 1223 K.

FTIR spectra of adsorbed CO₂ were collected with a Thermo Nicolet Nexus 470 spectrometer using a home-made stainless steel IR cell connected to a gas manifold. The cell had a path length of 10 cm and both ends were “capped” by IR-transparent NaCl windows. Catalyst samples of 20 mg were pressed into self-supported wafers of approximately 1 cm in diameter. These wafers were placed in a sample holder located at the center of the cell. Heating through the cell was provided by heating rods located in the sample holder and through a heating tape wrapped around the cell. The temperature was measured with a thermocouple placed in close proximity to the catalyst sample. Transmission spectra were collected with a resolution of 4 cm^{-1} (64 scans per spectrum).

Prior to each FTIR experiment, the samples were treated at 823 K for 1 h under flowing He. The cell was subsequently cooled down to 323 K in He and a stream containing a 45% CO₂/He mixture (80 ml/min) was introduced to the cell for 30 min. Following this step, the samples were purged with He at room temperature for 30 min to remove any remaining physisorbed CO₂, and the temperature was increased stepwise from 323 to 573 K (50–100 K steps). Each intermediate temperature was maintained constant for 30 min and during this period spectra were collected until no further changes were observed.

FTIR spectra were also collected at 433 K during the reaction of adsorbed 2'-hydroxyacetophenone with benzaldehyde. For these measurements the samples were first saturated with 2'-hydroxyacetophenone and subsequently the flow was switched to benzaldehyde, with spectra collected at different time intervals. Both reactants were brought in contact with He streams in satu-

rators maintained at 313 K and were introduced to the FTIR cell in the gaseous phase.

2.3. Catalytic activity measurements

Catalytic activity measurements were conducted in a home-made batch reactor system. The reactor was initially charged with 150 ml of a mixture containing 1.5 M benzaldehyde (Aldrich, 99+%) and 1.5 M 2'-hydroxyacetophenone (Aldrich, 99%) in DMSO (Alfa Aesar, 99.9%). After the reactor was charged, nitrogen was continuously bubbled through the system and the stirring rate was set to approximately 500 rpm. The reactor was then heated and the catalyst (165 mg; 60–80 mesh particles) was added when the temperature reached 433 K ($t = 0$). Following this point, the reactor was operated under total reflux. As shown previously [18], under these conditions the reactor is operating in the kinetic regime, and intrinsic rates can be calculated from the slope of the conversion vs. time curves obtained. Small samples (approximately 0.1 ml) were removed from the reactor periodically during the course of the reaction. These samples were diluted in isopropyl alcohol, separated from the solid catalyst through centrifugation, and analyzed off-line by gas chromatography (HP 5890; Restek RTX-1 capillary column; FID detector).

In order to rule out the possibility of leaching of Li from the catalyst samples into the reaction mixture, resulting in the onset of a homogeneous reaction route, a leaching test was performed for the 5 wt.% Li-modified sample. This sample was selected because it contained the highest amount of Li in the series of samples studied. No free Li was detected in the liquid phase after 90 min of reaction, as indicated by ICP measurements performed by Galbraith Labs. Furthermore, the reaction was also conducted under homogeneous conditions, using LiOH as the catalyst at a Li concentration equal to that present in the 0.1 wt.% Li-modified sample, which exhibited the highest initial reaction rates in our study. The catalytic activity observed in this case was minimal when compared to the activity observed during the measurements conducted with MgO and Li/MgO, indicating that even if some Li was leached, its contributions to the overall reaction rate can be neglected.

3. Results and discussion

3.1. Structure of Li-modified MgO samples

The surface areas of the different Li-modified MgO samples used in this study are shown in Table 1 and indicate a gradual decrease with increasing Li content. Such a decrease is consistent with pre-

Table 1
Characteristic results for several Li-modified MgO catalysts.

Samples Li content (wt.%)	S_{BET} (m^2/g)	Basicity (adsorbed $\mu\text{mol CO}_2/\text{m}^2$)				MgO crystallite size ^a (nm)
		Total	Weak	Medium	Strong	
0	27	9.5	2.7	5.5	1.3	22
0.05	23	11.9	4.3	6.2	1.4	ND
0.1	20	12.1	2.2	7.1	2.7	28
0.5	12	18.9	3.8	8.7	6.4	28
1	7	70.2	0.5	29.2	40.5	30
5	4	85.2	1.9	0.1	83.3	39

^a Calculations based on reflection at $2\theta = 42.8^\circ$.

vious literature reports, indicating a substantial sintering upon addition of alkali promoters to metal oxides, with the effect being magnified in the case of lithium-modified samples [24–26]. Diez et al. for example, synthesized MgO samples modified with group IA metals using solutions of their respective metal hydroxides. They suggested that the observed significant decrease of surface area was most likely due to a metal hydroxide phase blocking the MgO pores [25].

The X-ray diffraction patterns for some of the Li-modified MgO samples are shown in Fig. 1. The results indicate the presence of a single periclase phase of MgO in all samples, with characteristic diffraction peaks at 2θ of 37.1° , 42.8° , and 62.4° . Li_2CO_3 reflections also become visible in the diffraction patterns of the samples with Li contents higher than 0.1 wt.%. The presence of such Li_2CO_3 crystallites indicates a non-homogeneous distribution of lithium during the preparation, and could also explain, at least in part, the observed decrease of surface area with Li content, since such crystallites may be blocking the MgO pore structure.

The effect of lithium on the MgO crystallite size was also examined by considering the width of the main MgO reflection at $2\theta = 42.8^\circ$ corresponding to the (200) plane and by the use of the Scherrer equation. The results of these calculations are summarized in Table 1, and indicate that the crystallite size of MgO increases progressively with the addition of lithium, ranging from 22 nm for pure MgO to 39 nm for the 5 wt.% Li/MgO sample. A similar crystal-

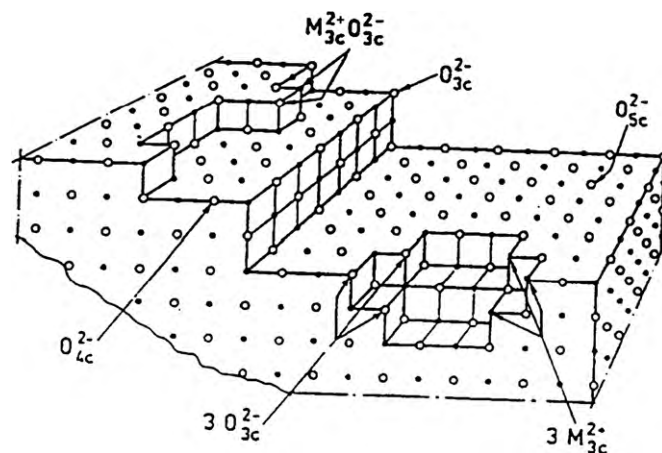


Fig. 2. MgO surface model proposed by Coluccia and Tench [27].

lite size increase was also observed previously upon modification of MgO with alkali promoters [26]. This increase in crystallite size with lithium loading also contributes to the decrease of surface area discussed above.

Fig. 2 shows a model for the MgO surface proposed by Coluccia and Tench [27]. Three types of O^{2-} sites are identified in this

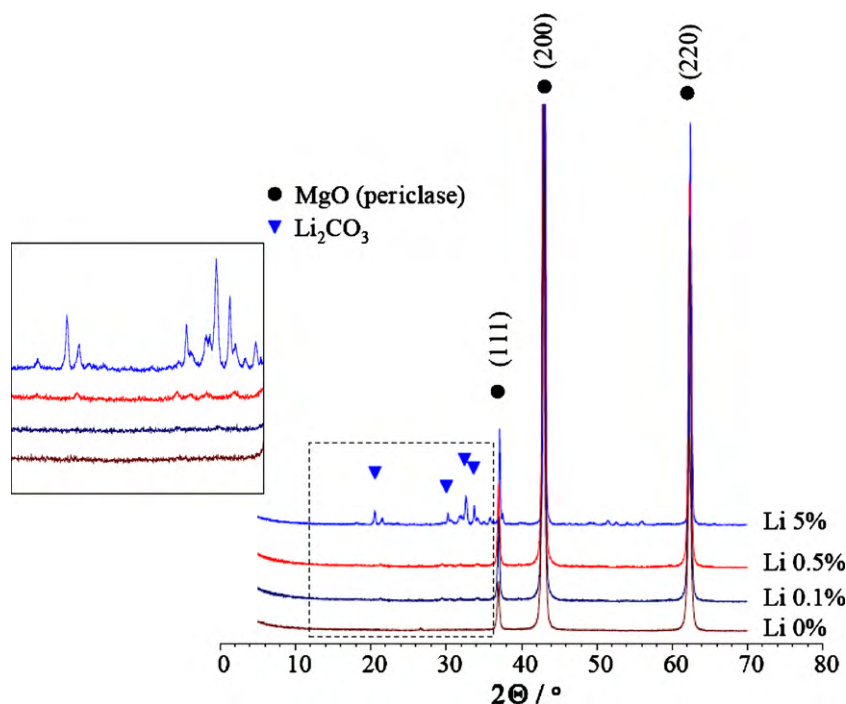


Fig. 1. X-ray powder diffraction patterns of different Li-modified MgO samples.

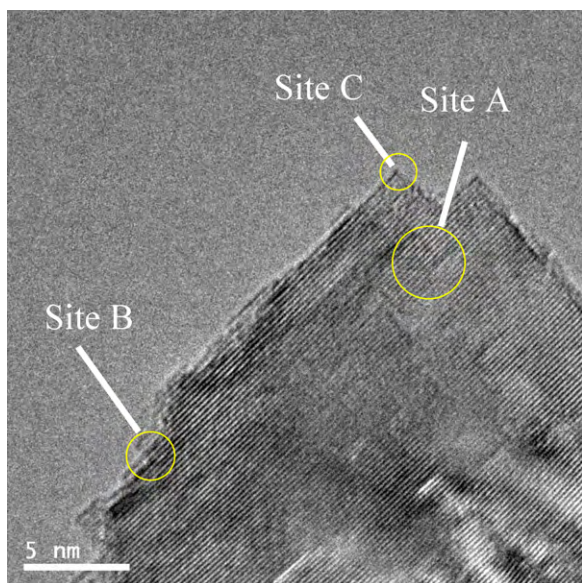


Fig. 3. HRTEM image of pure MgO with identified five-fold- (site A), four-fold- (site B), and three-fold- (site C) coordinated surface O^{2-} ions.

model: five-fold-coordinated O^{2-} sites (symbolized as O^{2-}_{5C}) in terraces, which are expected to be basic sites of medium strength; four-fold-coordinated O^{2-} sites (symbolized O^{2-}_{4C}) at edges, which are also expected to be basic sites of medium strength; and three-fold-coordinated O^{2-} sites (symbolized as O^{2-}_{3C}) at corners, which are expected to be basic sites of high strength, based on previous CO_2 adsorption measurements [28]. The nature of the basic sites generated is highly dependent on the pretreatment conditions.

Localization of such different types of coordinated O^{2-} sites is also visualized in the HRTEM images of our own samples, with an example shown in Fig. 3. Indeed, five-, four-, and three-fold-coordinated O^{2-} sites are identified in this image as “Site A”, “Site B”, and “Site C”, respectively. A visual comparison of the HRTEM images of pure and lithium-modified MgO samples is attempted in Fig. 4. A higher concentration of four- and three-fold-coordinated O^{2-} sites (i.e., edges and corners) is then apparent in the image of the 0.1 wt.% Li-modified sample as compared to the image of pure MgO.

3.2. Basicity of Li-modified MgO samples

The surface basicity of the different samples involved in this study was probed by CO_2 -TPD and FTIR measurements. The deconvoluted TPD profiles of CO_2 adsorbed on pure MgO, as well as MgO modified with different amounts of lithium are shown in Fig. 5. The quantified results obtained from the deconvolution of the TPD profiles are presented in Table 1. The TPD profile of pure MgO contains several CO_2 desorption peaks, indicating that a variety of basic sites of different strengths are present on the surface of this sample. The strength of such sites increases as the desorption in the TPD profile takes place at higher temperatures.

Upon introduction of lithium to MgO, the total basicity of the samples increases. Furthermore, several changes in the distribution of the basic sites can be observed in the TPD profiles. For example, the amount of medium strength basic sites with desorption peaks at 480 and 570 K increases with the lithium content, with the exception of the 5 wt.% Li sample, which shows almost no medium strength basicity. Furthermore, the surface concentration of the high strength basic sites (most likely low coordination oxygen anions) also increases with lithium content. These results are consistent with previous reports suggesting an increase in basic strength during modification of MgO with lithium [24,25]. Such an increase was attributed to the formation of lower coordination O^{2-} ions in Li-modified samples. We should point out that our structural characterization results described above do not allow us to determine the surface density of Li and to differentiate between Li cations present on the surface of MgO and Li cations occupying MgO lattice positions. Standard XPS measurements were not sufficient for such differentiation, due to sensitivity issues with samples containing less than 1 wt.% Li. Given the expected differences in the behavior of the oxygen anions associated with these sites, such information may have allowed us to be more specific regarding the changes observed in the amount of “medium” and “strong” basic sites. Nevertheless, the overall increase in the amount of both types of sites is the critical factor for the synthesis of flavanone, as discussed below.

In contrast to the “medium” and “strong” basic sites, the broad peak at 375 K corresponding to the “weak” basic sites (most likely bicarbonates formed on hydroxyl groups) was only slightly affected and no correlation was observed between the size of this peak and the lithium content in the different samples. Finally, a peak was also observed at temperatures above 973 K in the high Li-content samples. This peak can be attributed to the formation of bulk lithium carbonates in these samples and is not related to surface basicity.

The nature of the adsorbed CO_2 species formed was probed via FTIR measurements. Spectra of CO_2 adsorbed on pure and Li-

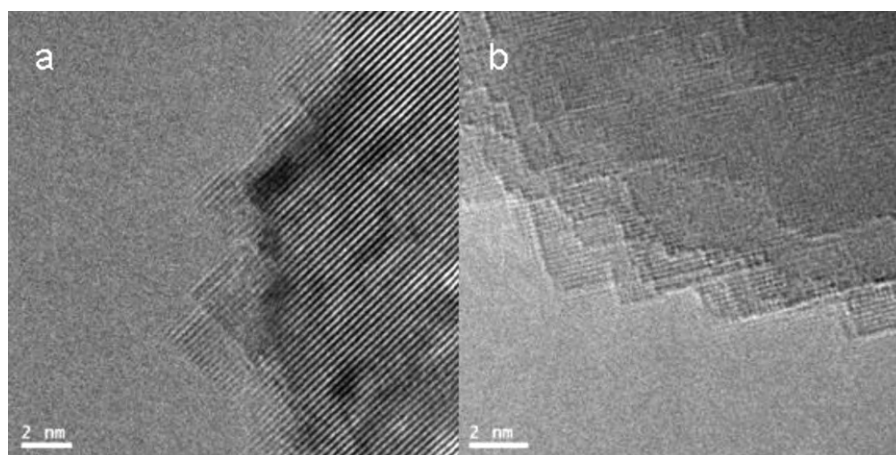


Fig. 4. HRTEM images of (a) pure MgO and (b) 0.1 wt.% Li-modified MgO.

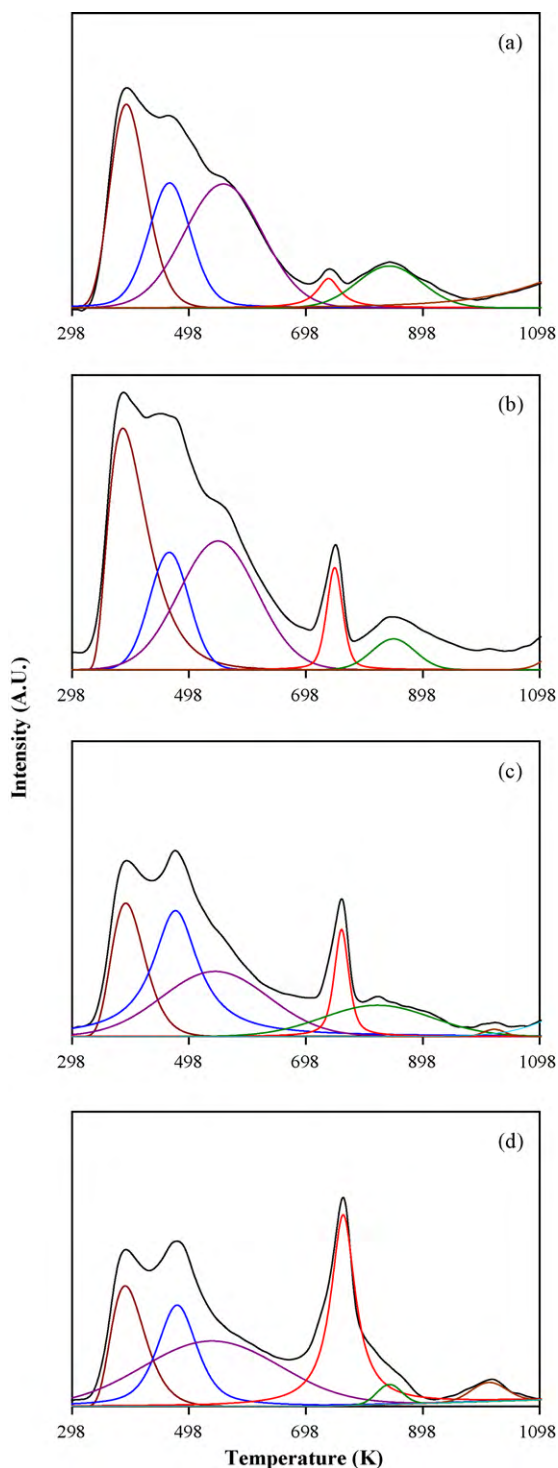


Fig. 5. CO₂-TPD profiles of: (a) MgO, (b) 0.05 wt.% Li/MgO, (c) 0.1 wt.% Li/MgO, and (d) 0.5 wt. % Li/MgO.

modified MgO samples at 323 K are shown in Fig. 6. The results indicate that CO₂ interacts mainly with O²⁻ and OH-sites and the nature of the carbonates formed is affected by the lithium content. In the case of pure MgO, six bands were observed at 1692, 1650, 1558, 1518, 1415, and 1223 cm⁻¹. Bands between 1400 and 1500 cm⁻¹ have been associated with the C–O stretching vibration [$\nu(\text{C–O})$] of carbonate ions [29]. Hence, we can assign the bands at 1415 and 1518 cm⁻¹ to unidentate carbonates (symmetric and asymmetric C–O stretching vibrations), most likely associated with

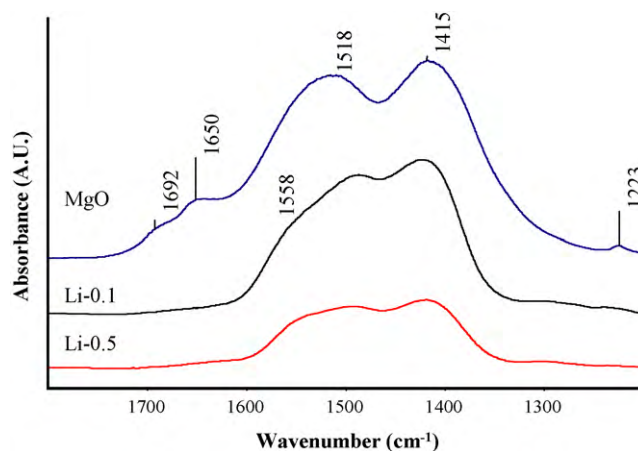


Fig. 6. FTIR spectra of CO₂ adsorbed at 323 K on pure and Li-modified MgO samples.

low (i.e., three-fold) coordination O²⁻ ions. The position of these bands shifts in the Li-modified samples to 1439 and 1495 cm⁻¹, respectively. This shift is likely due to the difference in electronegativity between Mg²⁺ and Li⁺. The difference ($\Delta\nu$) between the frequencies of the asymmetric and symmetric vibrations of surface carbonates has been associated with the partial charge of the surface oxygen to which the CO₂ is bonded [30]. In our case, this difference is reduced from 103 cm⁻¹ for pure MgO to 56 cm⁻¹ for the 0.1 wt.% Li-modified sample. This decrease can be attributed to the increase in electron-pair donor ability and the Lewis basic strength of the Li-modified samples.

The bands at 1692 and 1223 cm⁻¹ in the spectrum of pure MgO can be assigned to bicarbonate species associated with weak hydroxyl groups. Davydov et al. previously assigned bands at 1700 and 1220 cm⁻¹ to the asymmetric OCO stretching vibration [$\nu_{\text{as}}(\text{OCO})$] and the C–O [$\nu(\text{C–O})$] stretching vibrations respectively, of such bicarbonate species [31]. No bands associated with bicarbonates were observed in any of the Li-modified samples. Finally, the bands at 1558 and 1650 cm⁻¹ in the spectrum of pure MgO can be assigned to bidentate carbonates, which represent Lewis–Bronsted acid–base pairs, most likely found on edges and kinks.

Evacuation studies of CO₂ were also conducted to support these assignments. During these studies the bands at 1518 and 1415 cm⁻¹ remained the more predominant ones at temperatures up to 673 K. These bands also increased in intensity with the lithium content of the samples, suggesting a relationship between the formation of monodentate carbonates upon adsorption of CO₂ and the type of basic sites generated by Li modification. Furthermore, the relative intensities of these bands decreased at a slower rate with temperature in samples containing increasing amounts of lithium. These results suggest that lithium not only affects the density of basic sites but also their strength, as indicated by the CO₂ binding energy [26]. This is also consistent with the small shifts observed in the maxima of the desorption peaks corresponding to medium strength basic sites and the significant increase in the number of high strength basic sites, during CO₂-TPD measurements over the same set of Li-modified samples.

3.3. Catalytic activity for the synthesis of flavanone

2'-Hydroxyacetophenone conversions obtained over time in a batch reactor at 433 K with the pure, as well as the Li-modified MgO samples are shown in Fig. 7. The results are quantified in Table 2, where the calculated initial rates for the Claisen–Schmidt condensation reaction are presented normalized both per catalyst weight and surface area. The corresponding selectivities towards flavanone

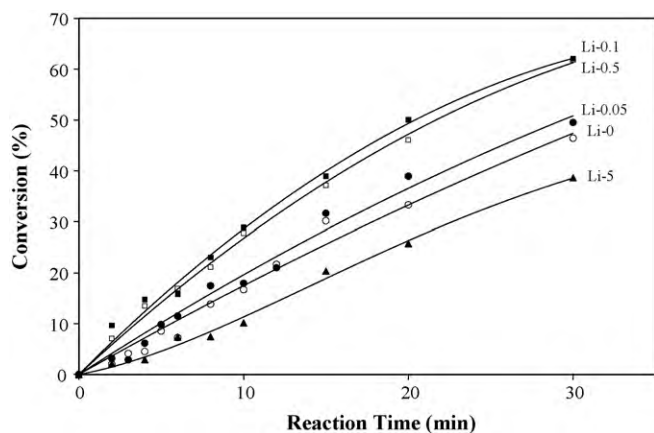


Fig. 7. 2'-Hydroxyacetophenone conversion as a function of time at 433 K. For detailed reaction conditions see Section 2.

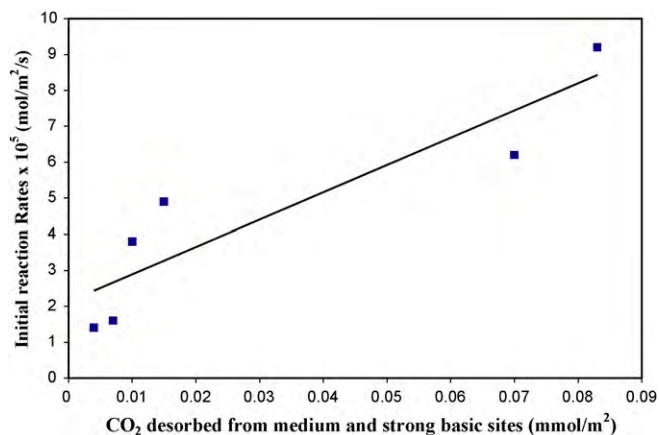


Fig. 9. Correlation of initial reaction rates for the Claisen-Schmidt condensation reaction with the amounts of CO₂ desorbed from pure and Li-modified MgO samples.

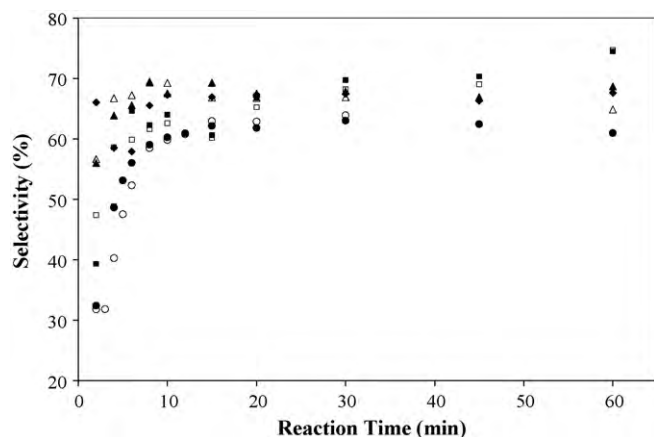


Fig. 8. Flavanone selectivity as a function of 2'-hydroxyacetophenone conversion obtained at 433 K over: (○) MgO, (●) 0.05 wt.% Li/MgO, (■) 0.1 wt.% Li/MgO, (□) 0.5 wt.% Li/MgO, (△) 1 wt.% Li/MgO and (▲) 5 wt.% Li/MgO. For detailed reaction conditions see Section 2.

as function of time are shown in Fig. 8. Flavanone selectivity values after 20 min of reaction time are also included in Table 2.

The results shown in Fig. 7 and Table 2 indicate that the rate of the Claisen-Schmidt condensation reaction is promoted by the presence of lithium at low lithium contents. Such a promotion is likely associated with the increased ability of the catalyst to abstract a proton from the phenolic group of 2'-hydroxyacetophenone, and to subsequently form a bond with the carbonyl group, a step that has been previously demonstrated to be important in the reaction mechanism [22,33]. Due to the similar atomic radii of Li and Mg, Mg²⁺ ions can be easily substituted by Li⁺ into the lattice. Following this process, Li⁺ ions tend to be localized on the surface in the form of Li⁺O⁻ groups with increased local electronegativity [32]. Consequently, the ability of such a surface to abstract a proton from

the hydroxyl group of 2'-hydroxyacetophenone is expected to be enhanced, which could in part explain the observed promotion of the initial reaction rates.

A maximum however, is observed on the weight-based catalytic activity with lithium content at 0.1 wt.% (Table 2). The decrease in the activity of samples containing more than 0.1 wt.% Li can be attributed to the significant loss of surface area, as evidenced by our BET and XRD measurements, and discussed in previous sections. In support of such a conclusion, the initial reaction rates normalized per unit surface area exhibit a continuous increase of the activity with lithium content (Table 2).

Finally, the results shown in Fig. 8 and Table 2 indicate that no significant differences in selectivity towards flavanone can be observed after 20 min of reaction among the different samples, including pure MgO, although the catalytic activities for these samples differ substantially. This result is consistent with our previous measurements, which suggest that the isomerization of 2'-hydroxychalcone to flavanone is significantly faster than the Claisen-Schmidt condensation. Hence, its rate is not affected by the Li modification of the MgO catalysts and the corresponding changes in basic site density and strength. A similar conclusion was also reached in our previous work focusing on the modification of MgO with different anions [23].

The catalytic behavior of the Li-modified MgO samples for the Claisen-Schmidt condensation reaction can be correlated to their surface basicity, and more specifically, the concentration of O²⁻ sites with different coordinations. As discussed previously, these O²⁻ sites can be either five-fold-coordinated when located on a flat surface, four-fold-coordinated when located at edges, or three-fold-coordinated when located at corners. The basic strength on these sites varies according to their coordination. As demonstrated in the TPD profiles shown in Fig. 5 and analyzed in Table 1, the basicity of the different samples was divided in three categories, designated as "weak", "medium", and "strong" basic sites. The "weak" basic sites are most likely associated with lattice-bound

Table 2
Catalytic activity of pure and Li-modified MgO samples for the synthesis of flavanone.

Samples (wt.% Li)	Claisen-Schmidt condensation rate		Flavanone selectivity (after 20 min) (%)
	(mol/g/s × 10 ⁴)	(mol/m ² /s × 10 ⁵)	
0	3.8	1.4	63
0.05	4.4	1.6	62
0.1	7.5	3.8	67
0.5	7.1	4.9	65
1	4.4	6.2	67
5	3.5	9.2	68

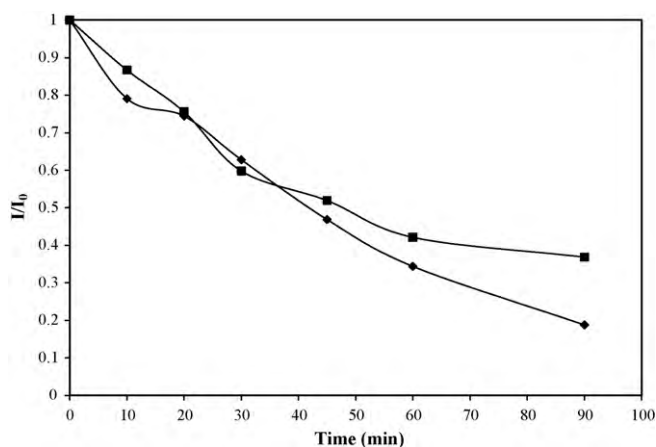


Fig. 10. Intensity of the 1368 cm^{-1} band of adsorbed 2'-hydroxyacetophenone during exposure of a saturated surface to benzaldehyde at 433 K: (■) MgO and (◇) 0.1 wt.% Li/MgO.

OH groups (i.e., Bronsted sites). The “medium” and “strong” sites are associated with four-fold- and three-fold-coordinated O^{2-} sites (i.e., Lewis sites). In the presence of lithium the number of both “medium” and “strong” basic sites increases substantially.

Fig. 9 shows the relationship between the initial reaction rates observed and the amount of “medium” and “strong” basic sites. Indeed, a good correlation exists between the initial reaction rates normalized per unit surface area and the amount of CO_2 desorbed from “medium” and “strong” basic sites. As discussed previously, this effect can be attributed to the ease of the deprotonation of 2'-hydroxyacetophenone, which is generally believed to be the first step of the Claisen–Schmidt condensation reaction mechanism [22,33].

3.4. FTIR study of the 2'-hydroxyacetophenone–benzaldehyde reaction

We have shown previously that upon adsorption of 2'-hydroxyacetophenone on MgO a characteristic band appears on the FTIR spectra at 1368 cm^{-1} and can be assigned to the CH_3 bending vibration of the corresponding surface phenolate ion formed [34,35]. This species reacts further with benzaldehyde as the Claisen–Schmidt condensation reaction proceeds towards the formation of 2'-hydroxychalcone. In situ spectra collected at 433K following the introduction of benzaldehyde onto pure and 0.1 wt.% Li-modified MgO samples saturated with 2'-hydroxyacetophenone are consistent with our previous results and indicate that the 1368 cm^{-1} band decreased steadily in intensity as the reaction between the surface phenolate ion and the benzaldehyde introduced took place. The change in the normalized intensity of the 1368 cm^{-1} band for both samples is shown as a function of time in Fig. 10.

The initial intensity of the 1368 cm^{-1} band was approximately 40% higher in the case of the Li-modified sample, indicating an increased ability of this sample to abstract a proton from the 2'-hydroxyacetophenone molecule upon adsorption, which is consistent with the discussion in the previous section regarding the role of lithium. However, the decrease in the intensity of the 1368 cm^{-1} band upon exposure to benzaldehyde is similar for both samples. Since this band previously remained unaffected under desorption conditions [22], this behavior indicates that a reaction takes place between the phenolate ion and benzaldehyde, as discussed in the previous paragraph. The results shown in Fig. 10 further suggest that the rate of this reaction is not significantly

affected by the introduction of lithium. Thus, the promotional effect exhibited by lithium is probably limited to the increased ability for abstracting a proton from 2'-hydroxyacetophenone during the initial adsorption.

4. Conclusions

Results obtained with MgO samples modified with different amounts of Li indicate a good correlation between Li content, surface basicity and the initial reaction rates for the Claisen–Schmidt condensation reaction, which represents the first step in the synthesis of flavanone. MgO undergoes structural changes upon modification with Li. At low lithium loadings, a higher concentration of surface defects becomes evident, with the 0.1 wt.% Li/MgO catalyst exhibiting a maximum in both defect concentrations and catalytic activity. The increase in activity is likely the result of the increased ability of Li-O^- pairs to abstract a proton from the 2'-hydroxyacetophenone molecule, which represents the first step of the adsorption and surface reaction processes that constitute the Claisen–Schmidt condensation mechanism. While this promotional effect is still present at higher Li loadings (i.e., above 0.1 wt.%), a substantial decrease in surface area becomes dominant in such samples, leading to lower overall weight-normalized reaction rates.

References

- [1] Y.-C. Hsiao, W.-H. Kuo, P.-N. Chen, H.-R. Chang, T.-H. Lin, W.-E. Yang, Y.-S. Hsieh, S.-C. Chu, *Chemico-Biological Interactions* 167 (2007) 193–206.
- [2] Y.J. Moon, X. Wang, M.E. Morris, *Toxicology In Vitro* 20 (2006) 187–210.
- [3] H.K. Kim, B.S. Cheon, Y.H. Kim, S.Y. Kim, H.P. Kim, *Biochemical Pharmacology* 58 (1999) 759–765.
- [4] V. Hernández, M.C. Recio, S. Mániz, R.M. Giner, J.-L. Ríos, *Life Sciences* 81 (2007) 480–488.
- [5] M. Comalada, I. Ballester, E. Bailón, S. Sierra, J. Xaus, J. Gálvez, F.S.d. Medina, A. Zarzuelo, *Biochemical Pharmacology* 72 (2006) 1010–1021.
- [6] Y. Takano-Ishikawa, M. Goto, K. Yamaki, *Phytomedicine* 13 (2006) 310–317.
- [7] K. Sakata, Y. Hirose, Z. Qiao, T. Tanaka, H. Mori, *Cancer Letters* 199 (2003) 139–145.
- [8] T. Guardia, A.E. Rotelli, A.O. Juárez, L.E. Pelzer, *Il Farmaco* 56 (2001) 683–687.
- [9] A.E. Rotelli, T. Guardia, A.O. Juárez, N.E. de la Rocha, L.E. Pelzer, *Pharmacological Research* 48 (2003) 601–606.
- [10] P. Tuchinda, V. Reutrakul, P. Claeson, U. Pongprayoon, T. Sematong, T. Santisuk, W.C. Taylor, *Phytochemistry* 59 (2002) 169–173.
- [11] B. Moulari, Y. Pellequer, H. Lboutounne, C. Girard, J.P. Chaumont, J. Millet, F. Muryard, *Journal of Ethnopharmacology* 106 (2006) 272–278.
- [12] L.E. Alcaráz, S.E. Blanco, O.N. Puig, F. Tomás, F.H. Ferretti, *Journal of Theoretical Biology* 205 (2000) 231–240.
- [13] A. Mantas, E. Deretey, F.H. Ferretti, M.R. Estrada, I.G. Csizmadia, *Journal of Molecular Structure: THEOCHEM* 504 (2000) 171–179.
- [14] D.N. Dhar, *The Chemistry of Chalcones and Related Compounds*, John Wiley & Sons, New York, 1981.
- [15] M.J. Climent, A. Corma, S. Iborra, J. Primo, *Journal of Catalysis* 151 (1995) 60–66.
- [16] M.T. Drexler, M.D. Amiridis, *Journal of Catalysis* 214 (2003) 136–145.
- [17] M.T. Drexler, M.D. Amiridis, *Catalysis Letters* 79 (2002) 175–181.
- [18] M.T. Drexler, M.D. Amiridis, *Catalysis of Organic Reactions*, Marcell Dekker Inc., 2000.
- [19] S.C. Hargrove-Leak, M.D. Amiridis, *Catalysis Communications* 3 (2002) 557–563.
- [20] S.C. Hargrove-Leak, J. Lichtenberger, M.D. Amiridis, *Catalysis of Organic Reactions*, CRC Press, 2005.
- [21] S.E. Blanco, J.J. Silber, G.E. Narda, L.J. Yamin, F.H. Ferretti, *Journal of Colloid and Interface Science* 180 (1996) 144–148.
- [22] J. Lichtenberger, S.C. Hargrove-Leak, M.D. Amiridis, *Journal of Catalysis* 238 (2006) 165–176.
- [23] Z. Liu, J.A. Cortes-Concepcion, M. Mustian, M.D. Amiridis, *Applied Catalysis A: General* 302 (2006) 232–236.
- [24] E.L. Jablonski, I.M.J. Vilella, S.C. Maina, S.R. de Miguel, O.A. Scelza, *Catalysis Communications* 7 (2006) 18–23.
- [25] V.K. Díez, C.R. Apesteguía, J.I. Di Cosimo, *Catalysis Today* 63 (2000) 53–62.
- [26] V.K. Díez, C.R. Apesteguía, J.I. Di Cosimo, *Journal of Catalysis* 240 (2006) 235–244.
- [27] S. Coluccia, A.J. Tench, in: 7th International Congress on Catalysis, Tokyo, 1980.
- [28] H. Hattori, *Applied Catalysis A: General* 222 (2001) 247–259.
- [29] K. Teramura, T. Tanaka, H. Ishikawa, Y. Kohno, T. Funabiki, *Journal of Physical Chemistry B* 108 (2004) 346–354.
- [30] R. Philipp, K. Fujimoto, *Journal of Physical Chemistry* 96 (1992) 9035–9038.
- [31] A.A. Davydov, N.A. Rubene, A.A. Budneva, *Kinetics and Catalysis* 19 (1978) 776.

- [32] H. Aitani, H. Yamada, T. Nishio, T. Shiono, S. Imamura, M. Kudo, S. Hasegawa, T. Tanaka, S. Yoshida, *Journal of Physical Chemistry B* 104 (2000) 10133.
- [33] A. Aguilera, A.R. Alcantara, et al., *Canadian Journal of Chemistry* 65 (1987) 1165–1171.
- [34] J. Palomar, J.L.G. De Paz, J. Catalan, *Chemical Physics* 246 (1999) 167–208.
- [35] W.A.L.K. Al-Rashid, M.F. El-Bermani, *Spectrochimica Acta Part A* 47 (1991) 35.